

A Precessing Ring Model for Low-Frequency Quasi-periodic Oscillations

Jeremy D. Schnittman^{1, 2}, Jeroen Homan², and Jon M. Miller³

ABSTRACT

We develop a simple physical model to describe the most common type of low-frequency quasi-periodic oscillations (QPOs) seen in a number of accreting black hole systems, as well as the shape of the relativistically broadened iron emission lines that often appear simultaneously in such sources. The model is based on an inclined ring of hot gas that orbits the black hole along geodesic trajectories. For spinning black holes, this ring will precess around the spin axis of the black hole at the Lense-Thirring (“frame-dragging”) frequency. Using a relativistic ray-tracing code, we calculate X-ray light curves and observed energy spectra as a function of the radius and tilt angle of the ring, the spin magnitude, and the inclination of the black hole. The model predicts higher-amplitude QPOs for systems with high inclinations, as seen in a growing number of black hole binary systems. We find that the *Rossi X-ray Timing Explorer* observations of low-frequency QPOs in GRS 1915+105 are consistent with a ring of radius $R \approx 10M$ orbiting a black hole with spin $a/M \approx 0.5$ and inclination angle of $i_{\text{BH}} \approx 70^\circ$. Finally, we describe how future X-ray missions may be able to use simultaneous timing and spectroscopic observations to measure the black hole spin and probe the inner-most regions of the accretion disk.

Subject headings: black hole physics – accretion disks – X-rays:binaries

1. INTRODUCTION

Over the past decade, X-ray timing and spectroscopy observations of accreting black hole binaries have provided us with increasingly sensitive measurements of the inner-most regions

¹Department of Physics, University of Maryland, 82 Regents Drive, College Park, MD 20742, schnittm@umd.edu

²Kavli Institute for Astrophysics and Space Research, Massachusetts Institute of Technology, 77 Massachusetts Avenue, Cambridge, MA 02139, jeroen@space.mit.edu

³Department of Astronomy, University of Michigan, 500 Church Street, Dennison 814, Ann Arbor, MI 48109, jonmm@umich.edu

of the accretion disk. With the proper theoretical understanding of these observations, we should be able to probe the behavior of matter and energy in the strongest known gravitational fields. Recent observations by Miller & Homan (2005) with the *Rossi X-ray Timing Explorer (RXTE)* provide time-varying measurements of spectroscopic features for a black hole on sub-second time scales. They find a strong correlation between the phase of the light curve oscillation and the width of the iron K α emission line.

We propose a simple model to explain this correlation and make a number of additional predictions for the spectral features and light curves of similar black hole binary systems. The quasi-periodic oscillations (QPOs) considered in this paper are so-called “type C” QPOs, following the naming convention described in Remillard et al. (2002). These appear to be the most common type of QPO in black hole binaries; they are seen in the spectrally hardest states, are stronger and more coherent than types A and B, and are observed over a large range in frequency (typically between ~ 0.1 Hz and ~ 10 Hz), even within a single source. It is believed that this type of black hole QPO is related to the 10-60 Hz QPOs observed in many neutron star low-mass X-ray binaries (Wijnands & van der Klis 1999; Casella, Belloni, & Stella 2005).

Stella & Vietri (1998) suggested for these 10–60 Hz neutron star QPOs that their frequencies might correspond to the Lense-Thirring frequency of test particles around a spinning neutron star. A later version of their model was also applied to low-frequency QPOs in black hole X-ray binaries (Stella, Vietri, & Morsink 1999). In this work we expand on that model, using a fully relativistic ray-tracing model, and for the first time compute quantitative X-ray light curves and emission line spectra that may be compared more directly with observations. This is similar to the ray-tracing analysis described in Schnittman & Bertschinger (2004) for the hot spot model of high frequency QPOs. However, that hot spot model, which was developed primarily to explain the 3:2 ratio in the frequencies of QPO peaks, requires that the emission comes from a specific radius in the disk where the coordinate frequencies have small integer ratios (Abramowicz & Kluzniak 2001; Abramowicz et al. 2003). The precessing ring model presented in this paper requires no such special radius, consistent with observations, where the LFQPOs are seen to drift in frequency (and thus radius), while the pairs of high frequency QPOs are always seen at the same frequency within a given source (McClintock & Remillard 2005).

One of the primary objections to the interpretation of QPOs in the context of gravitomagnetic frame-dragging is based on the Bardeen-Petterson effect (Bardeen & Petterson 1975), which predicts that the inner regions ($r \lesssim 100M$) of a viscous accretion disk should align perpendicular to the black hole spin axis. If the disk is constrained to the black hole equatorial plane, then the Lense-Thirring precession will not produce a time-varying light

curve, as the observed orientation of the disk does not change. However, subsequent theoretical studies of the inner accretion disk have led to a number of different scenarios in which the emitting gas could have a significant inclination relative to the black hole spin axis. These perturbations could be driven by trapped pressure gradients (Kato & Honma 1991; Ipser 1996), radiation warping (Ipser & Petterson 1990; Pringle 1996; Maloney, Begelman, & Pringle 1996; Maloney & Begelman 1997), or gravitomagnetic forces (Markovic & Lamb 1998). Markovic & Lamb (1998) argue that the radiation warping modes will be strongly damped, while the lowest-order gravitomagnetic modes, corresponding to the Lense-Thirring precession frequency, will be weakly damped and should exhibit quality factors of $Q \sim 2-50$, in agreement with observations.

In the context of the supermassive black hole in Sgr A*, Rockefeller, Fryer, & Melia (2005) have recently shown that for hot, magnetized disks with low Mach-numbers, internal pressure gradients can sustain large-scale, coherent precession of the entire inner-disk region. This picture of a hot, geometrically thick region in the inner disk is consistent with some of the earliest models of black hole accretion disks (Thorne & Price 1975), as well as more recent general relativistic magneto-hydrodynamic simulations that predict a local density maximum, or “inner torus” just outside the inner-most stable circular orbit (De Villiers & Hawley 2003; De Villiers, Hawley, & Krolik 2003). Additionally, the fact that most black hole QPOs appear predominately in the power-law dominant spectral states and usually show greater amplitudes at higher energies further suggests that they are originating from a hot, non-thermal region of the accretion flow. For the purposes of this paper, we are not concerned with the exact physical mechanism that produces the precessing ring, but rather we are interested in the observational manifestation of such a ring, assuming that it exists.

In Section 2 we describe in greater detail the features of the precessing ring model and the global disk geometry. We also show the relation between black hole spin and ring radius for a given QPO frequency. Section 3 presents the results of our ray-tracing calculation, giving light curves and iron line widths for a range of model parameters. In Section 4 we compare these results to a number of black hole systems with type C QPOs, in particular the GRS 1915+105 observations of Miller & Homan (2005). In Section 5 we conclude with a discussion of how this model may be tested further with future X-ray missions and observations of active galactic nuclei (AGN).

2. DESCRIPTION OF THE MODEL

For the basic geometry of this model, we consider a circular ring made up of massive test particles on geodesic orbits around a Kerr black hole. This ring can be thought of as

a stream of hot gas with finite thickness, emitting X-rays isotropically in the *RXTE/PCA* energy band ($\sim 2 - 60$ keV). We assume that the majority of the observed high-energy flux, including the broadened iron emission line, is produced by this hot ring. In order to produce a fluorescent line from non-ionized iron, it may be best to think of the ring as a relatively cool thermal emitter, surrounded by a hot corona that produces the power-law flux seen in observations. However, we note that a hot ring may well have multiple ionization states, which could complicate the analysis of the broadened iron emission line.

Unlike a number of theoretical models for the integer ratios seen in high-frequency QPOs, which require specific geodesic frequencies, here there is no special radius required for the ring to form. In other words, given the black hole mass and spin, a ring of a specific radius will precess at one particular frequency, but there is nothing physically special about that radius or frequency, consistent with the fact that the low-frequency QPOs tend to drift in frequency from one observation to the next. Yet just like the high-frequency QPO models, the ring model will be sensitive to viewer inclination angle i_{BH} (measured from the black hole spin axis), preferentially selecting high (edge-on) inclinations.

The ring axis is inclined at some angle $\Delta\theta$ to the black hole spin equator (see Fig. 1 for a schematic diagram of the ring geometry), and thus undergoes Lense-Thirring precession due to the dragging of inertial frames around the Kerr black hole (Bardeen & Petterson 1975). This misalignment could be caused by one of two basic mechanisms: (1) the binary orbit of the donor star and the outer accretion disk are aligned with the black hole spin axis ($i_{\text{BH}} = i_{\text{bin}}$), and some instability (such as those mentioned in the Introduction) causes the inner disk to be perturbed and form a ring inclined with respect to the orbital plane; or (2) the entire binary orbit is misaligned with the black hole spin ($i_{\text{BH}} = i_{\text{bin}} \pm \Delta\theta$), so that the inner accretion flow is forced to precess around the spin axis. In either case, the precessing ring will appear to a distant observer with an inclination angle that varies periodically, thus modulating the observed X-ray light curve.

The Lense-Thirring precession frequency ν_{LT} is a function of the black hole mass M , spin a , and the radius R of the ring. Specifically, ν_{LT} is the difference between the vertical and azimuthal coordinate frequencies, which for nearly circular prograde orbits can be written as (Bardeen, Press, & Teukolsky 1972; Perez et al. 1997; Merloni et al. 1999)

$$\nu_{\text{LT}} = \nu_{\phi} - \nu_{\theta} = \frac{1}{2\pi} \left(\frac{1}{R^{3/2} + a} \right) \left[1 - \left(1 - \frac{4a}{R^{3/2}} + \frac{3a^2}{R^2} \right) \right]^{1/2}, \quad (1)$$

where we have adopted geometrized units with $G = c = M = 1$. To convert to cgs units, simply multiply ν_{LT} by $2.04 \times 10^5 (M/M_{\odot})^{-1}$ Hz.

Using the compact binary system of GRS 1915+105 as an example, in Figure 2 we show

how the radius of the ring is a function of black hole spin and measured QPO frequency. Fixing the black hole mass at $14.4M_{\odot}$ (Harlaftis & Greiner 2004), we plot the radius at which a ring would have a given precession frequency ν_{LT} , as a function of black hole spin. For example, a spin of $a/M = 0.5$ would give $\nu_{\text{LT}} = 1$ Hz at a radius of $R = 12.5M$ and $\nu_{\text{LT}} = 2$ Hz at $R = 9.5M$. Also plotted are the corresponding orbital frequencies ν_{ϕ} for geodesic orbits at the given radii. For smaller spins, the ring must be closer to the black hole to experience the same frame-dragging effects, and thus it has a higher orbital frequency. In the limit of $a/M \rightarrow 0$, the required radius moves inside that of the inner-most stable circular orbit (ISCO), and is not considered physical. From this argument alone, the precessing ring model gives a modest lower limit on the black hole spin of $a/M \gtrsim 0.1$ for GRS 1915+105. For “typical” black hole binaries with $M \approx 10M_{\odot}$ and $\nu(\text{LFQPO}) \approx 10$ Hz (McClintock & Remillard 2005), this lower limit would be $a/M \gtrsim 0.25$.

The entire model can thus be described completely with a few basic parameters: the black hole mass M , spin a , and inclination angle i_{BH} , the ring’s radius R , and the tilt angle $\Delta\theta$. The characteristic thickness (cross-sectional radius) of the ring is taken as $\delta R/R = 0.1$, but for moderately thick rings ($\delta R/R \lesssim 1/3$), we find the results to be largely independent of this parameter. As shown in Figure 2, for a given black hole mass and QPO frequency, the spin can be determined by measuring the radius R . In the next Section we show how the light curves and iron emission lines can be used to infer R , as well as the angles i and $\Delta\theta$.

As in the hot spot QPO model described in Schnittman (2005), the width of the QPO peaks is caused by the finite lifetime of coherent rings, as they are continually formed and destroyed and formed again with random phases. This leads naturally to a Lorentzian peak in the power spectrum with a full-width half-maximum inversely proportional to the characteristic coherence lifetimes of the inclined rings. One of the predictions of the finite-lifetime model is that the higher harmonic peaks should have the same widths as the fundamental (Schnittman 2005), in agreement with observations of GRS 1915+105 (Morgan, Remillard, & Greiner 1997; Miller & Homan 2005). With this model, the observed Q -values of $\sim 6 - 8$ correspond to typical ring lifetimes of $\sim 2 - 3$ precessional periods.

3. LIGHT CURVES AND IRON LINE SPECTRA

The simulated light curves of the precessing ring were created using a fully relativistic ray-tracing code for the Kerr metric (Schnittman & Bertschinger 2004). As with the hot spots and arcs described in that paper, here we consider primarily an optically thin line emission model, where the gas is an isotropic, monochromatic emitter in the local rest frame

of the “guiding center” geodesic orbits. Future work will investigate the effects of other, more sophisticated emission and absorption models (Schnittman & Rezzolla 2005).

Even though the effective inclination of the ring will change purely sinusoidally at a single frequency ν_{LT} , the light curve can have significant power at higher harmonics due to relativistic beaming and gravitational lensing effects (Schnittman & Bertschinger 2004). These higher harmonics are clearly seen in the power spectra of many type C QPOs, typically weaker in power by about an order of magnitude (Morgan, Remillard, & Greiner 1997; Miller & Homan 2005), consistent with the light curves calculated below for black hole inclinations of $60 - 70^\circ$.

In Figure 3 we show a series of snap-shots of how the precessing ring would appear to a distant observer, for a representative spin of $a/M = 0.5$ and radius $R = 9.5M$. The black hole inclination is $i_{\text{BH}} = 70^\circ$ and the tilt angle is $\Delta\theta = 20^\circ$. The images are color-coded by relative intensity on a logarithmic scale. The gas orbiting the black hole is moving towards the observer on the right side of each image, and moving away on the left side, respectively giving the blue-shifted and red-shifted spectral peaks plotted in the lower right of each frame. For both the light curves (plotted in the lower left of each frame) and energy spectra, the vertical axis is normalized intensity in units of [$\# \text{ photons/s/cm}^2$].

At the peak of the light curve (frame “c” in Fig. 3), the effective inclination is $i_{\text{eff}} = i_{\text{BH}} + \Delta\theta = 90^\circ$, resulting in a flux maximum due to both special relativistic beaming and the formation of an Einstein ring through the gravitational lensing of the emission from the far side of the black hole. This lensing produces a third, intermediate spectral peak from the gravitational magnification of gas moving transverse to the observer’s line of sight (Beckwith & Done 2004; Schnittman & Rezzolla 2005). While this third peak is most pronounced at very high inclinations where lensing is more important, it should also be observable for $i_{\text{eff}} \approx 70^\circ$ (frames “b” and “d”) with a next-generation X-ray spectroscopy mission.

Due in large part to these relativistic effects, the amplitudes of the observed QPOs are primarily sensitive to the angles i_{BH} and $\Delta\theta$. The effective inclination as a function of time can be written

$$i_{\text{eff}}(t) = i_{\text{BH}} + \Delta\theta \cos(\nu_{\text{LT}} t + \psi), \quad (2)$$

where ψ is some arbitrary phase. Understandably, the greater the range of i_{eff} , the greater the QPO amplitude. However, because of the planar symmetry around $i_{\text{eff}} = 90^\circ$, which maps $i_{\text{eff}} \rightarrow (180^\circ - i_{\text{eff}})$, systems with very high i_{BH} actually produce smaller light curve modulations for the same $\Delta\theta$. Additionally, for edge-on systems with $i_{\text{BH}} = 90^\circ$, symmetry dictates that the light curve is modulated primarily at frequency $2\nu_{\text{LT}}$, with no power at the fundamental ν_{LT} (Bursa et al. 2004).

Figure 4 illustrates this dependence by plotting the simulated rms amplitude as a function of black hole inclination for a range of tilt angles $\Delta\theta$. We set fixed the spin $a/M = 0.5$ and ring radius $R = 9.5M$, corresponding to $\nu_{\text{LT}} = 2$ Hz for $M = 14.4M_{\odot}$. For a given tilt angle $\Delta\theta$, we see that the greatest amplitude fluctuations occur when $i_{\text{BH}} + \Delta\theta = 90^{\circ}$. For example, if $i_{\text{BH}} = 80^{\circ}$ and $\Delta\theta = 20^{\circ}$, then the effective range of i_{eff} is only $[60^{\circ}..90^{\circ}]$, while for $i_{\text{BH}} = 70^{\circ}$ the range extends to $[50^{\circ}..90^{\circ}]$, giving a larger light curve modulation. We find that the rms amplitude is relatively insensitive to the black hole spin, being slightly larger for smaller values of the spin parameter and thus ring radius. In the paradigm where the binary orbit is aligned with the black hole spin ($i_{\text{BH}} = i_{\text{bin}}$), a thick outer accretion disk may obscure some of the emission for $i_{\text{bin}} \gtrsim 80^{\circ}$, limiting the potential range of observations (Narayan & McClintock 2005). Yet if the outer disk is misaligned with the black hole axis (see below, Section 4), the ring could be unobsured even for very large values of i_{BH} .

As can be seen clearly from the frames of Figure 3, the effective inclination affects not only the total observed intensity, but also significantly changes the shape of the relativistic emission line. With our current level of spectroscopic and timing sensitivity, the detailed features of these spectra can not be discerned on the QPO time scale. Yet, as shown in Miller & Homan (2005), the emission line width and centroid may be measurable with sufficient accuracy to constrain the precessing ring model.

Following that approach, in Figure 5 we plot the line centroid E_{avg} and width (standard deviation) ΔE as a function of black hole spin, for a fixed inclination of $i_{\text{BH}} = 70^{\circ}$ and QPO frequency of 2 Hz. In order to best understand these results, recall Figure 2, which shows the dependence of orbital frequency ν_{ϕ} on spin. For a given QPO frequency ν_{LT} , smaller values of the spin correspond to smaller radius rings and thus larger orbital velocities. As ν_{ϕ} increases, so does the relativistic Doppler broadening, as the emitting gas is moving faster, both towards and away from the observer.

While the gravitational red-shift at smaller radii reduces the energy of all emitted photons equally, giving an observed E_{avg} lower than the rest frame energy, special relativistic beaming causes the observer to see a larger number of blue-shifted photons (through the invariance of I_{ν}/ν^3), thus *increasing* E_{avg} . At high inclinations ($i_{\text{eff}} \gtrsim 70^{\circ}$) the beaming factor dominates, giving larger values of E_{avg} at smaller radii (spin value), while at lower inclinations ($i_{\text{eff}} \lesssim 70^{\circ}$) the gravitational red-shift wins out and reduces E_{avg} for smaller spins. The upper curves (above the dashed line) in Figure 5a are taken at the light curve maximum, corresponding to the highest effective inclination, while the lower curves have successively smaller values of i_{eff} and thus smaller E_{avg} .

The width of the emission line ΔE , shown in Figure 5b, is a direct measurement of the range of Doppler shifts seen by the observer. As the effective inclination increases, the gas

moves towards and away from the observer with higher velocity, broadening the line more. However, in the limit of $i_{\text{eff}} \rightarrow 90^\circ$, while the greater beaming helps broaden the line, the lensing effects actually serve to *decrease* the width ΔE as the gravitational magnification amplifies the contribution of a small region of the ring, giving the central third peak of the iron line spectrum (see Fig. 3c). Therefore the line properties E_{avg} and ΔE are nearly identical for $i_{\text{eff}} \approx 80^\circ - 90^\circ$, as can be seen in the top three curves in Figures 5a and 5b. Of course, higher resolution observations of these lines could break the inclination degeneracy by giving detailed spectral features other than just E_{avg} and ΔE .

As a point of comparison, we show in Figure 6 the same iron line predictions for an inclination angle of $i_{\text{BH}} = 30^\circ$. As in Figure 5, we see that the range of E_{avg} and ΔE are greater at small spin values where the orbital velocities are larger. However, due to the smaller inclination angle, relativistic beaming plays a significantly smaller role, so the gravitational redshift dominates the behavior of E_{avg} at small spin and radius (Fig. 6a). Similarly, the nearly face-on projection gives a much smaller range of redshift around the ring, corresponding to smaller values of ΔE (Fig. 6b).

By measuring the iron line profiles at the maxima and minima of the QPO light curve, we have another method for potentially determining a black hole’s spin. As can be seen in Figures 5a and 6a, larger values of the spin parameter correspond to a smaller range in E_{avg} between maximum and minimum intensity. While the range in E_{avg} is also sensitive to $\Delta\theta$, we can use measurements of ΔE to break this degeneracy: the difference between $\Delta E(\text{max})$ and $\Delta E(\text{min})$ is nearly independent of spin for $a/M \gtrsim 0.3$, so measuring this difference should give a robust measurement of $\Delta\theta$. Then with this value for $\Delta\theta$, we can use the line centroids plotted in Figure 5a to determine the spin. However, even this simple method can be plagued by systematic errors described in the following Section.

4. COMPARISON WITH OBSERVATIONS

One of the predictions of our model that can be tested with current instrumentation (*RXTE*) is that type C QPOs should in general be stronger in sources with a higher inclination angle (see Fig. 4). We made a first attempt to test this prediction by selecting black hole X-ray transients with well-known binary inclinations that have shown type C QPOs in *RXTE* data. At present, there are only a handful of sources that meet both criteria, with just two sources (4U 1543–47 and GX 339–4) having relatively well-determined low inclinations. In Table 1 we list the sources included in our survey. We have included one source, XTE J1650–500, whose inclination is somewhat uncertain but might fill in the gap between the high inclination ($i_{\text{bin}} \gtrsim 70^\circ$) and low inclination ($i_{\text{bin}} \lesssim 30^\circ$) sources. In an effort to

compare similar QPO modes, we have selected *RXTE* observations in which these sources showed type C QPOs that were either close to 1–1.5 Hz or close to 4.5–5 Hz, since we could not identify a single frequency that was observed in all sources. Of course, this is quite reasonable considering the range of black hole masses and (presumably) spins involved, i.e. the same values of R/M correspond to a range of precession frequencies in different sources.

For all of the sources, we constructed Poisson-subtracted power spectra using data from the entire PCA bandpass (2–60 keV), following methods described in Homan et al. (2005). The power spectra were fit with combinations of broad and narrow Lorentzians, and the rms values quoted in Table 1 were calculated by integrating the narrow Lorentzians over frequency from 0 to ∞ Hz. The QPOs had Q -values between 4 and 11.5. The quoted QPO frequencies correspond to the frequency at which the Lorentzian reaches its maximum in $\nu P(\nu)$, where $P(\nu)$ is the power in units of $[(\text{rms}/\text{mean})^2/\text{Hz}]$. In order to provide a visual comparison with the precessing ring model, in Figure 7 we reproduce the data from Table 1, plotting QPO-rms versus binary inclination for these seven sources. Although our dataset is arguably limited, there are clear indications that the rms amplitudes are indeed higher in the sources with the highest inclinations, and are roughly in agreement with the results shown in Figure 4. In most cases one or more harmonics were detected, but in the two sources with the lowest inclinations (4U 1543–47 and GX 339–4), those features were very weak, in agreement with the model predictions.

Assuming that the *RXTE* light curves come primarily from the hot ring emission, we can use the QPO amplitudes to constrain the accretion geometry of the system. Again using GRS 1915+105 as an example, we take the inclination of the outer disk as the binary inclination, given by Fender et al. (1999) as $i_{\text{bin}} = 66^\circ \pm 2^\circ$. For the QPO near 2 Hz, the observed rms amplitude is 13.6% (Miller & Homan 2005). As mentioned in Section 2, there are two basic options for the global geometry of the system. If the black hole spin axis is aligned with the binary system’s orbital angular momentum, then $i_{\text{BH}} = 66^\circ$ and from Figure 4 we infer that $\Delta\theta \approx 17^\circ$. If, on the other hand, the precession is caused by a global misalignment of the outer disk and the spin axis, then the binary inclination can be understood as the minimum of the effective inclination: $i_{\text{bin}} = i_{\text{eff}}(\text{min}) = i_{\text{BH}} - \Delta\theta = 66^\circ$. In this scenario, Figure 4 shows that $i_{\text{BH}} \approx 80 - 85^\circ$ and $\Delta\theta \approx 15 - 20^\circ$ is consistent with an rms of 13.6%. However, at least for the case of GRS 1915+105, the lower level of harmonic power ($\sim 10\%$ of the fundamental) seems to point to the first scenario, with the disk and spin axis aligned, since a spin inclination of $i_{\text{BH}} \gtrsim 80^\circ$ would produce a light curve with harmonic power roughly equal to that of the fundamental.

Constraining the broad iron line predictions of the ring model with the current *RXTE* energy spectra has proven somewhat more difficult. For GRS 1915+105, Miller & Homan

(2005) find that the iron line is significantly broader at the light curve maximum compared to the minimum, measuring the FWHM as 2.7 and 1.1 keV, respectively. This corresponds to our ΔE values of 1.1 and 0.5 keV, in qualitative but not quantitative agreement with Figure 5b. If, however, we were to set $i_{\text{BH}} = 46^\circ$ and $\Delta\theta = 20^\circ$, and thus $i_{\text{bin}} = i_{\text{eff}}(\text{max}) = 66^\circ$, the predicted values of ΔE would closely fit the observed values for $a/M \gtrsim 0.5$. Yet this geometry would give significantly smaller QPO power in the fundamental, and almost no power in the first harmonic, in disagreement with the data.

At the same time, the observed values of E_{avg} are actually *lower* for the light curve maximum, with $E_{\text{avg}}(\text{max}) = 6.3$ keV and $E_{\text{avg}}(\text{min}) = 6.7$ keV, disagreeing qualitatively with the predictions of our model (see Fig. 5a). This might be due in part to systematic factors that complicate direct comparison of theory and observation. There may very well be significant contributions from other ionization state of iron in the inner disk, as well as contributions to the energy spectrum from other elements, which could artificially increase or decrease the location of the line center E_{avg} , as determined by fitting a single Gaussian peak. While this other emission could also serve to artificially broaden the line, including iron $\text{K}\alpha$ emission from other, less relativistic regions of the disk would have the opposite effect of narrowing the observed line, *decreasing* the measured value of ΔE .

With the quality of present data, we believe that the precessing ring model should be able to give good constraints on the overall geometry of the inner accretion region from the light curve amplitudes and harmonics. On the other hand, the spectral resolution currently available is not high enough to use the iron lines to constrain the model parameters or effectively measure the black hole spin. Perhaps simultaneous observations could use the timing capabilities of *RXTE* to measure the QPO amplitudes and thus i_{BH} and $\Delta\theta$, while the high-resolution spectroscopy of *XMM-Newton* or *Chandra* could give more detailed measurements of the iron lines, even if they must be averaged over the QPO period.

5. DISCUSSION AND CONCLUSIONS

We have developed a geodesic precessing ring model to help explain the properties of type C low-frequency QPOs in black hole binaries. In this model, the surrounding accretion disk may be slightly misaligned with the black hole spin axis (as would generally be the case for compact binaries), or the inner-most region of the disk may get excited into an inclined orbit, forming a ring of hot gas precessing around the black hole spin axis at the Lense-Thirring frequency. For a given QPO frequency, we have shown the dependence of the ring's radius on the black hole spin, which gives a lower limit on the spin parameter, assuming the ring must be outside of the ISCO. Using a relativistic ray-tracing code, we

have produced X-ray light curves and time-varying iron line emission spectra. Similar to the hot spot model described in Schnittman & Bertschinger (2004), the ring model predicts the QPO amplitudes should increase with increasing inclination, in agreement with observations. Another important feature predicted by this model is the existence of a third, intermediate peak in the broad iron line spectrum at the QPO phase corresponding to maximum intensity, formed by the gravitational lensing of emission from the far side of the black hole.

In the states where most of the type C QPOs are observed, the emission of black hole X-ray binaries in the *RXTE* band is usually dominated by two spectral components: a soft thermal component that probably comes from the accretion disk and a hard power-law component. This hard component has often been associated with the inverse-Compton scattering of thermal photons through a corona of hot electrons, and more recently also with emission from the base of a jet (Markoff et al. 2003). However, the existence of QPOs in the radio-faint observations of GRS 1915+105 suggests that they do not originate in a jet (Miller & Homan 2005). Type C QPOs, and in fact many types of QPOs in X-ray binaries, have often been associated with this hard spectral component—not only because the fractional amplitude of the QPOs increases with energy, but also because the QPOs are detected in energy bands where the contribution from the disk is negligible. In view of these facts, it seems clear that while the disk may determine the seed frequencies, it is likely that some other geometry is also involved in producing the non-thermal component and the QPO behavior. For example, it has long been proposed that the inner-most section of a thin accretion disk may be very hot, optically thin, and thus radiatively inefficient (Thorne & Price 1975). We assume this medium of hot gas is closely aligned with the inner edge of the accretion disk, which in our model takes the form of a geodesically precessing ring.

The GRS 1915+105 observations of Miller & Homan (2005) can be explained well with the precessing ring model, matching the observed amplitudes of the fundamental and harmonic peaks of the QPO power spectrum. The rms variations of 13 – 15%, coupled with an independently measured inclination of $i_{\text{BH}} = i_{\text{bin}} = 66^\circ$ (Fender et al. 1999), suggest a tilt angle of $\Delta\theta \approx 15 - 20^\circ$. The spectral line measurements suggest a moderate to high spin with $a/M \gtrsim 0.5$ so that $\Delta E \lesssim 1.5$ keV, but the *RXTE* spectral data does not have enough energy resolution to rule out lower values of a/M . In short, our ring model agrees quite well with the light curve modulations, giving good estimates for the overall geometry of the system, yet the poor spectral data still cannot sufficiently constrain the black hole spin a/M .

Until recently, only time-averaged iron emission line profiles, and lines drawn from flux windows during aperiodic variability, had been studied with moderate and high resolution spectrometers. The recently launched *Suzaku* and future missions such as *Constellation-X*

and *XEUS* promise high spectral resolution along with high effective area. This is exactly the combination required to rigorously test the predictions of our precessing ring QPO model.

Suzaku X-ray Imaging Spectrometer (XIS) observations of GRS 1915+105 for \sim 100 ksec in states similar to those considered by Miller & Homan (2005) should achieve the same flux sensitivity as obtained with *RXTE* but with a spectral resolution ten times higher (\sim 100 eV versus \sim 1 keV at 6 keV). This may be sufficient to clearly detect a third peak in the iron emission line profile using the same QPO-phase-resolved technique. Depending on their final configurations, *Constellation-X* and *XEUS* may be able to achieve the same flux sensitivity as the Miller & Homan (2005) result in only a few ksec (assuming similar QPO amplitudes and frequencies), with an energy resolution of a few eV at 6 keV. With such observatories, a third peak in the iron emission line profile, if present, should be clearly resolved. Indeed, with *Constellation-X* and *XEUS*, it may be possible to detect a modulation of the iron line flux and profile in as few as 100 QPO cycles, which would enable detailed measurements of the inner disk ring evolution with time.

While this paper has focused primarily on stellar-mass black holes, and a single source in particular, the ring model could easily be applied to AGN observations as well. In fact, the much longer time scales associated with AGN would greatly improve our spectral resolution by using “slower” observatories like *Chandra* and *XMM-Newton*. Since the spin of an AGN is thought to come primarily from accretion, it is likely the accretion disk and black hole spin axes are closely aligned, potentially giving a small tilt $\Delta\theta$ and thus little variation in the light curve. Also, the massive accretion disk around an AGN is almost certainly optically thick, decreasing the relative effects of gravitational lensing (photons cannot pass through the disk and form Einstein rings). However, due to the larger signal-to-noise ratio for AGN timing observations, no QPOs have yet been unambiguously identified in AGN, making a direct comparison to galactic black holes more difficult.

We thank Chris Reynolds for helpful discussions and Cole Miller for his extensive and constructive comments to an early version of the manuscript. JDS is grateful to Ed Bertschinger for his continued insights and encouragement. Support comes from NASA grant NAG5-13306.

REFERENCES

Abramowicz, M. A., & Kluzniak, W. 2001, A&A 374, L19
Abramowicz, M. A., Karas, V., Kluzniak, W., Lee, W. H., & Rubesco, P. 2003, PASJ 55, 467

Bardeen, J. M., & Petterson, J. A. 1975, ApJ 195, L65

Bardeen, J. M., Press, W. H., Teukolsky, S. A. 1972, ApJ 178, 347

Beckwith, K., & Done, C. 2004, MNRAS, 352, 353

Bursa, M., Abramowicz, M. A., Karas, V., & Kluzniak, W. 2004, ApJ, 617, L45

Casella, P., Belloni, T., & Stella, L. 2005, ApJ, 629, 403

De Villiers, J.-P., & Hawley, J. F. 2003, ApJ, 592, 1060

De Villiers, J.-P., Hawley, J. F., & Krolik, J. H. 2003, ApJ, 599, 1238

Fender, R. P., et al. 1999, MNRAS, 304, 865

Greene, J., Bailyn, C. D., & Orosz, J. A. 2001, ApJ, 554, 1290

Harlaftis, E. T., & Greiner, J. 2004, A&A, 414, L13

Homan, J., Miller, J. M., Wijnands, R., van der Klis, M., Belloni, T., Steeghs, D., & Lewin, W. H. G. 2005, ApJ, 623, 383

Iping, R. C., & Petterson, J. A. 1990, A&A, 239, 221

Ipser, J. R. 1996, ApJ, 458, 508

Kato, S., & Honma, F. 1991, PASJ, 42, 95

Maloney, P. R., Begelman, M. C., & Pringle, J. E. 1996, ApJ, 472, 582

Maloney, P. R., & Begelman, M. C. 1997, ApJ, 491, L43

Markoff, S., Nowak, M., Corbel, S., Fender, R., & Falcke, H. 2003, New Astronomy Review, 47, 491

Markovic, D., & Lamb, F. K. 1998, ApJ, 507, 316

McClintock, J. E., & Remillard, R. A. 2005, in *Compact X-ray Sources*, ed. W. H. G. Lewin & M. van der Klis, preprint [astro-ph/0306213]

Merloni, A., Vietri, M., Stella, L., & Bini, D. 1999, MNRAS, 304, 155

Miller, J. M., & Homan, J. 2005, ApJ, 618, L107

Morgan, E. H., Remillard, R. A., & Greiner, J. 1997, ApJ, 482, 993

Narayan, R., & McClintock, J. E. 2005, *ApJ*, 623, 1017

Orosz, J. A., et al. 2002, *ApJ*, 568, 845

Orosz, J. A. 2003, *IAU Symposium*, 212, 365

Orosz, J. A., McClintock, J. E., Remillard, R. A., & Corbel, S. 2004, *ApJ*, 616, 376

Perez, C. A., et al. 1997, *ApJ*, 476, 589

Pringle, J. E. 1996, *MNRAS*, 281, 357

Remillard, R. A., Sobczak, G. J., Munoz, M. P., & McClintock, J. E. 2002, *ApJ*, 564, 962

Rockefeller, G., Fryer, C. L., & Melia, F. 2005, accepted to *ApJ*, preprint [astro-ph/0507302]

Schnittman, J. D., & Bertschinger, E. 2004, *ApJ*, 606, 1098

Schnittman, J. D. 2005, *ApJ*, 621, 940

Schnittman, J. D., & Rezzolla, L. 2005, submitted to *ApJ*, preprint [astro-ph/0506702]

Stella, L., & Vietri, M. 1998, *ApJ*, 492, L59

Stella, L., Vietri, M., & Morsink, S. M. 1999, *ApJ*, 524, L63

Thorne, K. S., & Price, R. H. 1975, *ApJ*, 195, L101

Wijnands, R., & van der Klis, M. 1999, *ApJ*, 514, 939

Wu, K., Soria, R., Hunstead, R. W., & Johnston, H. M. 2001, *MNRAS*, 320, 177

Table 1: QPO-rms measurements for seven black hole X-ray binaries with different inclinations

Source	Inclination (degrees)	QPO frequency (Hz)	QPO rms (%)	Ref.	<i>RXTE</i> Obs. ID
4U 1543–47	20.7 ± 0.5	4.49 ± 0.05	6.5 ± 0.5	1	70128-01-01-00
GX 339-4	15–30	4.78 ± 0.09	7.2 ± 1.2	2	70110-01-95-00
		1.24 ± 0.01	5.9 ± 0.5		70109-01-06-00
XTE J1650–500	$>50 \pm 3$	4.67 ± 0.03	5.8 ± 0.3	3	60113-01-12-03
		1.31 ± 0.14	$5.0_{-0.4}^{+0.6}$		60113-01-05-00
H1743–322	60–70	4.75 ± 0.01	9.98 ± 0.13	4	80146-01-03-00
GRS 1915+105	66 ± 2	1.04 ± 0.01	11.3 ± 0.1	5	20402-01-50-01
GRO J1655–40	70.2 ± 1.2	1.35 ± 0.01	19.3 ± 0.3	6	91502-01-01-13
XTE J1550–564	72 ± 5	4.73 ± 0.01	11.7 ± 0.2	7	30191-01-28-01
		1.04 ± 0.01	15.8 ± 0.3		30188-06-01-03
		1.54 ± 0.01	15.8 ± 0.3		30188-06-04-00

References: 1. Orosz (2003) 2. Wu et al. (2001) 3. Orosz et al. (2004)

4. Homan et al. (2005) 5. Fender et al. (1999) 6. Greene et al. (2001)

7. Orosz et al. (2002)

Fig. 1.— Schematic diagram of the inclined ring geometry. The ring has a major radius R , cross-sectional radius δR , and is inclined at an angle $\Delta\theta$ with respect to the black hole equator. The observer is located at an inclination i_{BH} with respect to the black hole spin axis, giving an effective inclination to the ring axis of $i_{\text{eff}} = i_{\text{BH}} \pm \Delta\theta$.

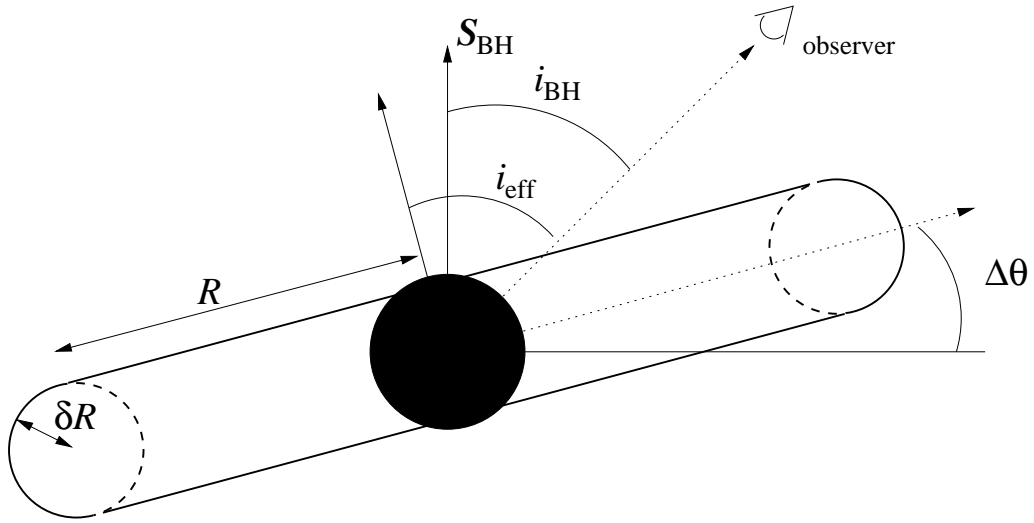


Fig. 2.— Orbital radius (*solid lines*) at which the Lense-Thirring precessional frequency is equal to the frequency of the QPO peaks for GRS 1915+105, located near 1 and 2 Hz (*thick and thin lines, respectively*), as a function of black hole spin a/M (assuming a mass of $14.4M_\odot$). We only consider cases where this radius is outside of the inner-most stable circular orbit (R_{ISCO}), shown here by a dotted line. Also plotted (*dashed lines*) are the corresponding Keplerian frequencies ν_ϕ for circular geodesic orbits at the given radius.

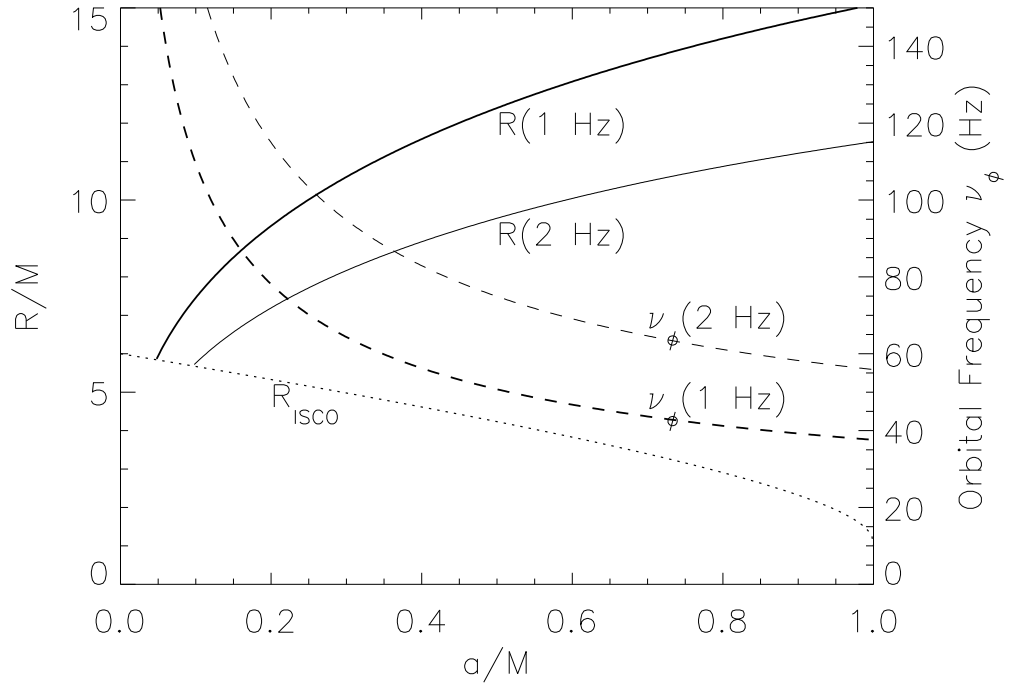


Fig. 3.— Ray-traced images of the precessing ring model, shown at various phases of the Lense-Thirring period. Also shown is the integrated X-ray light curve (*lower left*) and the broadened emission line spectrum (*lower right*) for each frame. The black hole has a spin of $a/M = 0.5$, inclination of $i_{\text{BH}} = 70^\circ$, and the ring tilt angle is $\Delta\theta = 20^\circ$, giving effective inclinations of $i_{\text{eff}} = 50^\circ, 70^\circ, 90^\circ$, and 70° in the four frames shown. This geometry is characterized by three distinct peaks in the spectrum, due to the photons beamed away from the observer on the left, towards the observer on the right, and a middle peak from the gravitational magnification of gas moving transverse relative to the observer.

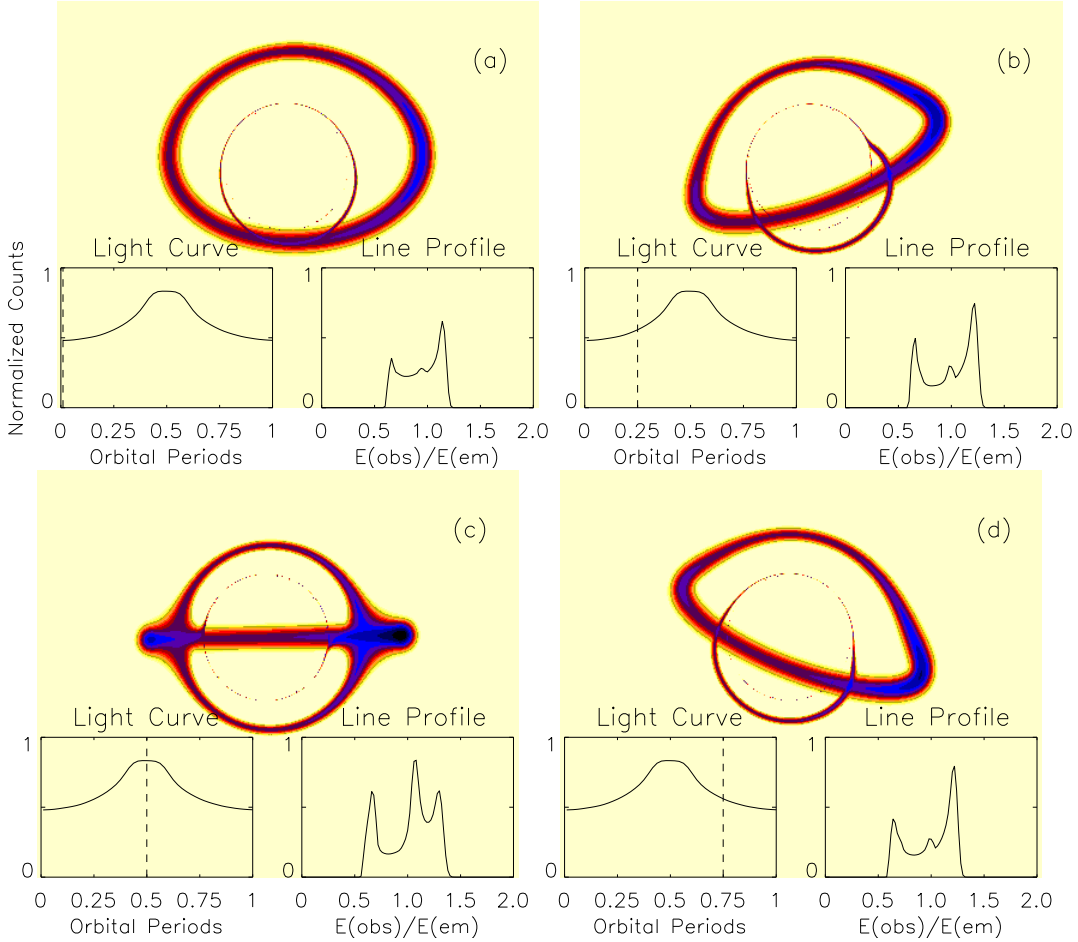


Fig. 4.— QPO amplitude of the X-ray light curve fluctuations as a function of the inclination angle i_{BH} of the black hole spin axis. The ring precesses around the spin axis with a tilt angle of $\Delta\theta$, giving an effective range of inclinations of $i_{\text{eff}} = i_{\text{BH}} \pm \Delta\theta$. The black hole has spin $a/M = 0.5$ and the ring has radius $R = 9.5M$.

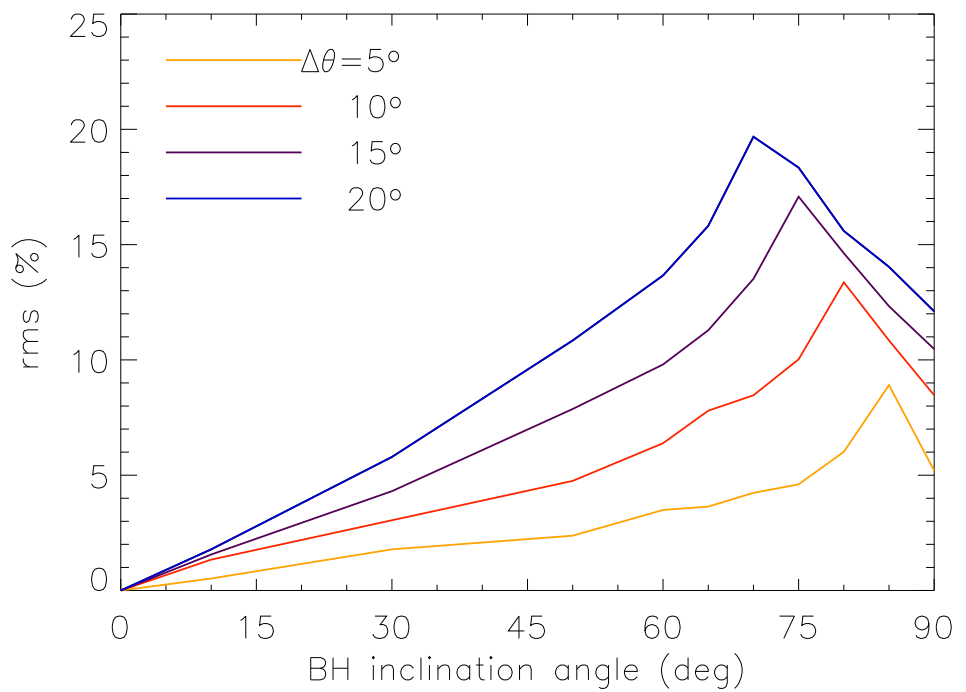


Fig. 5.— (a) Center of relativistically shifted iron emission line E_{avg} as a function of black hole spin, for an inclination angle of $i_{\text{BH}} = 70^\circ$ and radius of $R = 9.5M$. (b) The line widths ΔE for the same broadened emission lines. For both plots, the spectra are taken at the phases corresponding to the light curve minima (*below dashed curve*) and maxima (*above dashed curve*).

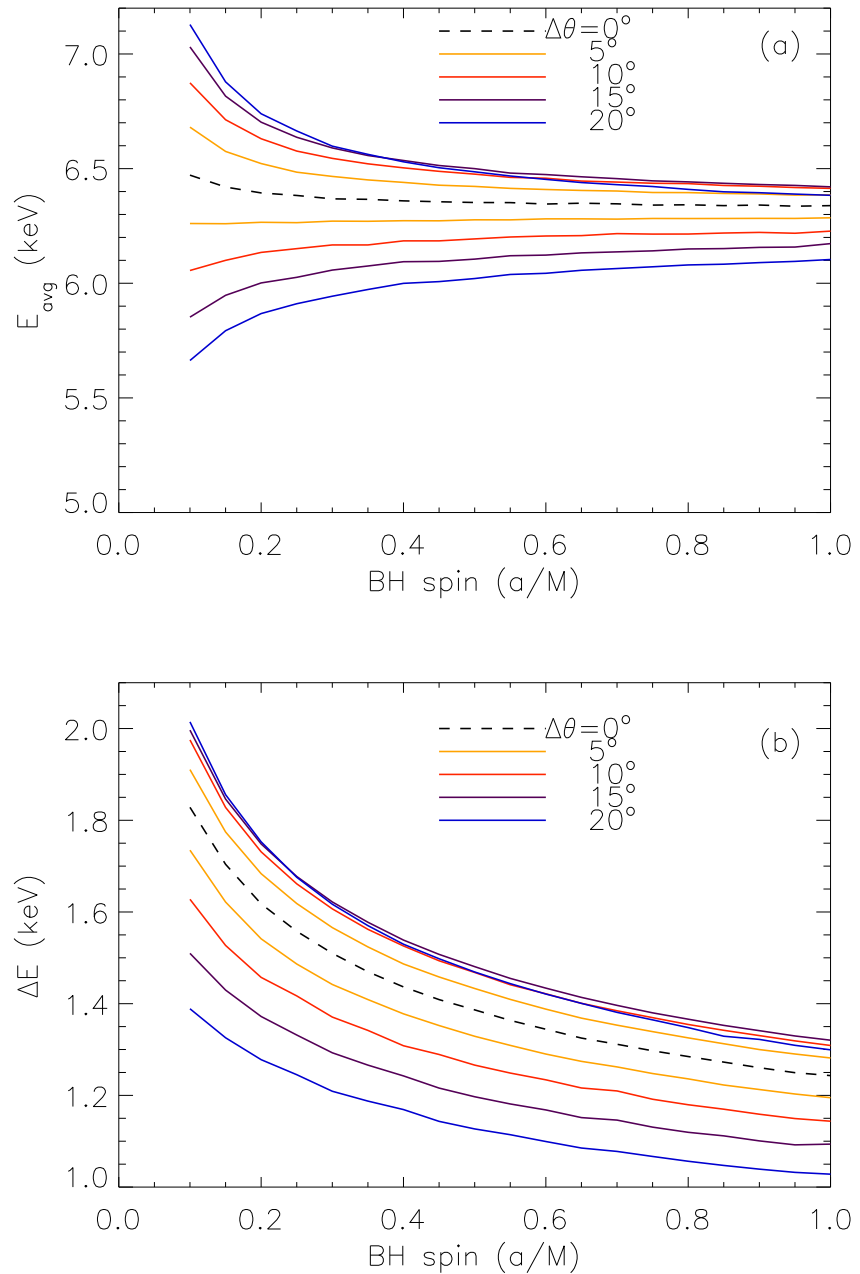


Fig. 6.— (a) E_{avg} and (b) ΔE as in Figure 5, but for a black hole inclination of $i_{\text{BH}} = 30^\circ$. For both plots, the spectra are taken at the phases corresponding to the light curve minima (*below dashed curve*) and maxima (*above dashed curve*). Note that the top curves in each of these plots correspond directly to the bottom curves in Figure 5: $i_{\text{eff}}(\text{min}) = i_{\text{BH}} - \Delta\theta = 70^\circ - 20^\circ$ and $i_{\text{eff}}(\text{max}) = i_{\text{BH}} + \Delta\theta = 30^\circ + 20^\circ$.

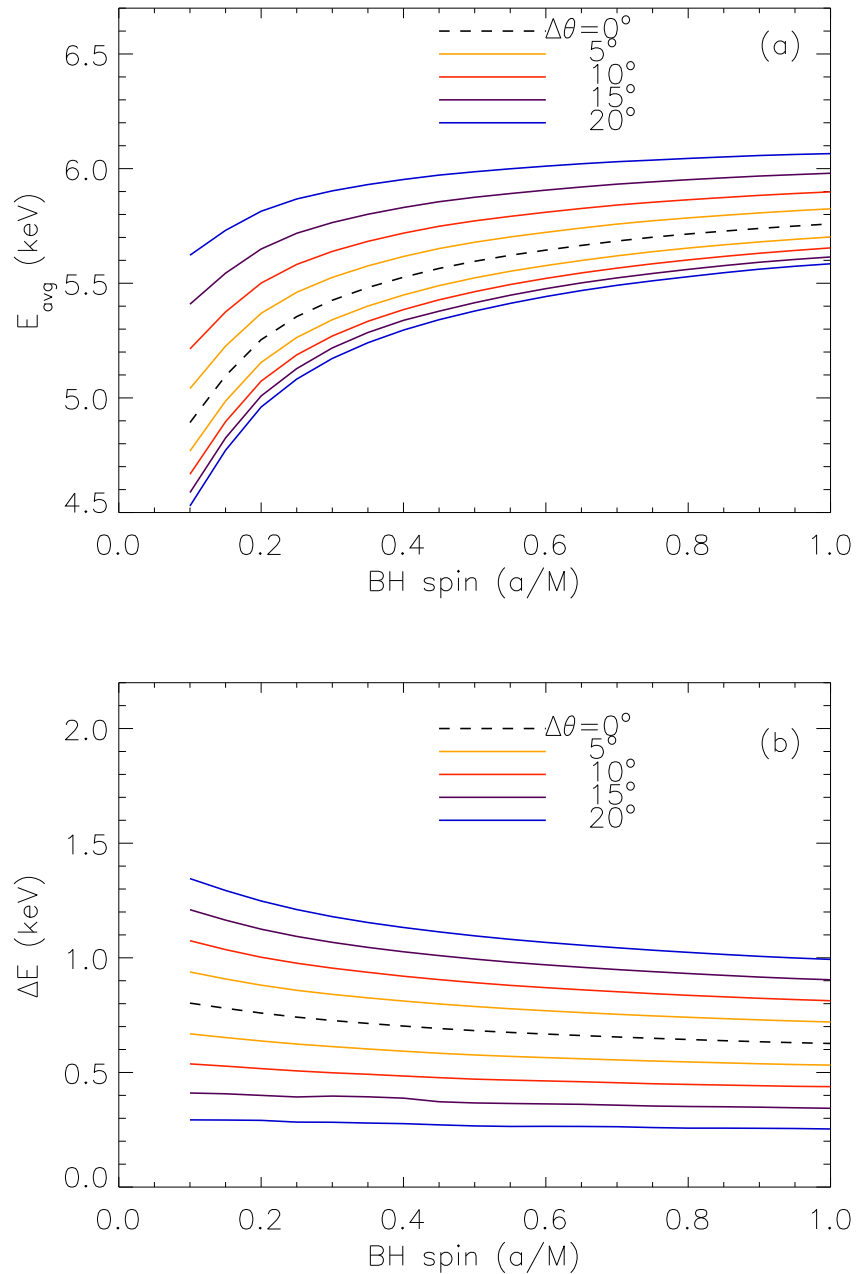


Fig. 7.— Dependence of rms amplitude on inclination for the black hole X-ray binaries listed in Table 1. The figure shows type C QPOs observed in the frequency ranges 1-1.5 Hz (*squares*) and 4.5-5 Hz (*circles*). For XTE J1650–500, arrows indicate the lower limit on the inclination. As predicted in Figure 4, the data shows a clear trend that suggests higher-inclination systems will have higher-amplitude QPOs.

